Biosensors and Bioelectronics 68 (2015) 210–217

Contents lists available at ScienceDirect

Biosensors and Bioelectronics

journal homepage: www.elsevier.com/locate/bios

Fluorescence sensing of chromium (VI) and ascorbic acid using graphitic carbon nitride nanosheets as a fluorescent "switch"

Mingcong Rong [a], Liping Lin [a], Xinhong Song [a], Yiru Wang [a], Yunxin Zhong [c], Jiawei Yan [c], Yufeng Feng [d], Xiuya Zeng [d], Xi Chen [a,b,*]

[a] Department of Chemistry and the MOE Key Laboratory of Spectrochemical Analysis & Instrumentation, College of Chemistry and Chemical Engineering, Xiamen University, Xiamen 361005, China
[b] State Key Laboratory of Marine Environmental Science, Xiamen University, Xiamen 361005, China
[c] Department of Chemistry, College of Chemistry and Chemical Engineering, Xiamen University, Xiamen 361005, China
[d] the First Affiliated Hospital of Xiamen University, Xiamen University, Xiamen 361005, China

ARTICLE INFO

Article history:
Received 28 August 2014
Received in revised form
2 December 2014
Accepted 8 December 2014
Available online 16 December 2014

Keywords:
Cr(VI)
g-C_3N_4 nanosheets
On–off–on fluorescence sensing
Inner filter effect (IFE)
AA

ABSTRACT

Using graphitic carbon nitride (g-C_3N_4) nanosheets, an effective and facile fluorescence sensing approach for the label-free and selective determination of chromium (VI) (Cr(VI)) was developed. The fluorescence of the solution of g-C_3N_4 nanosheets was quenched effectively by Cr(VI) via the inner filter effect. Under optimal conditions, a wide detection linear range for Cr(VI) was found to be from 0.6 μM to 300 μM with a limit of detection (LOD) of 0.15 μM. In addition, the fluorescence of the solution of g-C_3N_4 nanosheets-Cr(VI) could be sensitively turned on in the presence of a reductant such as ascorbic acid (AA) via an "on–off–on" fluorescence response through the oxidation–reduction between Cr(VI) and AA. And a wide detection linear range for AA was found to be from 0.5 μM to 200 μM with an LOD of 0.13 μM. Furthermore, the proposed method has the potential application for detection of Cr(VI) in lake waters and AA in biological fluids.

1. Introduction

In our daily life, chromium is a widely used industrial material, including in the metallurgy, electroplating, tanning industries and the production of pigment dyes, plastics, protective coating and ceramics (Rattanarat et al., 2013; Ščančar and Milačič, 2014). Generally, chromium exists primarily in two stable oxidation states, trivalent chromium (Cr(III)) and hexavalent chromium (Cr(VI)). Cr(III) is an essential trace element for humans and plays an important role in insulin action and glucose, lipid and protein metabolism. However, Cr(VI) is high carcinogenic and can cause damage to the human respiratory, gastrointestinal, immunological, hematological, reproductive and developmental systems. Because of its highly soluble character, Cr(VI) is mobile and biologically available in ecosystems (Broadhurst and Domenico, 2006; Sedman et al., 2006). For these reasons, it is vitally important to develop methods for the sensitive and selective detection of Cr(VI). Up to now, many methods and materials have been used to detect Cr(VI), including UV–vis spectrophotometry (Balasubramanian, 1999; Ravindran et al., 2012; Zhao et al., 2012), surface plasmon field-enhanced resonance light scattering method (Han et al., 2007), electrochemical technique (Jin et al., 2014; Li and Lin, 2006), fluorescence sensors (Hosseini et al., 2012; Sun et al., 2013; Zheng et al., 2013), inductively coupled plasma-mass spectrometry (Wang et al., 2010), chromatography (Arancibia et al., 2003), inductively couple atomic emission spectrometry (Balasubramanian, 1999) and atomic absorption spectroscopy (Chwastowska et al., 2005). Although these methods are highly sensitive, most of them suffer disadvantages such as expensive cost, time-consuming, a complicated pretreatment process and the operation of sophisticated instruments, which limit their wide application. Ascorbic acid (AA) is an important antioxidant playing a vital role in the diet of humans and is used for the prevention and treatment of the common cold, mental illness, infertility, AIDS and cancer (Hernández et al., 2006; Li and Lin, 2006). In recent years, many methods have been explored for the determination of AA based on complicated chemical modified materials (Chen and Yan, 2009; Ishii et al., 2011; Jahan et al., 2014; Li et al., 2014; Malashikhina and Pavlov, 2012). Therefore, exploring novel, highly fluorescent, inexpensive and eco-friendly nanomaterials to detect Cr(VI) and AA using simple and convenient fabrication are urgently needed.

Graphitic carbon nitride (g-C_3N_4) is a typical metal-free polymeric semiconductor, which exhibits structural similarity to graphene but with different properties. Because of its unique physical

* Corresponding author. Fax: +86 592 2184530.
E-mail address: xichen@xmu.edu.cn (X. Chen).

http://dx.doi.org/10.1016/j.bios.2014.12.024
0956-5663/

and chemical properties, both bulk g-C_3N_4 and g-C_3N_4 nanosheets have received worldwide attention and are applied extensively in sensing (Cheng et al., 2012, 2013; Lee et al., 2010; Tang et al., 2014; Xu et al., 2014), drug delivery and cancer imaging (Lin et al., 2014a; Zhang et al., 2014c, 2013), oxygen reduction reaction (Huang et al., 2014; Ma et al., 2014a), water splitting (Hou et al., 2014; Zhang et al., 2014a), peroxidase-like catalysis of hydrogen peroxide (Lin et al., 2014b; Tian et al., 2013b, 2013c) and photocatalytic organics degradation (Li et al., 2013; Zhu et al., 2014). In addition, both theoretical and applied studies confirm that g-C_3N_4 with atomic-scale thickness and nanoscale size can greatly promote the photoresponse and electroresponse in contrast with bulk materials owing to its high specific surface area (Huang et al., 2014; Ma et al., 2014b; Niu et al., 2012; Yang et al., 2013; Zhang et al., 2013). There are a series of solutions aimed at preparing atomic-scale thickness g-C_3N_4 nanosheets. The most commonly used methods include liquid phase exfoliation (Yang et al., 2013; Zhang et al., 2013), chemical oxidation (Chen et al., 2013; Xu et al., 2013) and hydrothermal method (Zhang et al., 2014b, 2014c). Meanwhile, the fluorescent sensors based on g-C_3N_4 nanosheets have increased rapidly. For example, a rapid and ultrasensitive approach for the determination of Cu^{2+} based on the florescence change of ultrathin g-C_3N_4 nanosheets is reported by Sun et al. (Tian et al., 2013a). The intensively long-persistent luminescence property of g-C_3N_4 nanosheets is found and reported, and g-C_3N_4 nanosheets are applied as turn-on persistent luminescence probes in the imaging detection of biothiols in biological fluids (Tang et al., 2013). Similarly, it is reported that g-C_3N_4 nanosheets-MnO_2 sandwich nanocomposite serves as a novel turn-on fluorescence sensing material for rapidly and selectively imaging detection of glutathione in living cells (Zhang et al., 2014d).

In our study, with the chemically oxidized and liquid exfoliated g-C_3N_4 nanosheets, we developed a facile and effective fluorescence "on–off" sensing approach for the label-free selective detection of Cr(VI) based on the inner filter effect (IFE) and a fluorescence "on–off–on" strategy for the determination of AA via the oxidation–reduction between Cr(VI) and AA. The developed approach provided a wide linear range and a low detection limit for the determination of Cr(VI) and AA.

2. Materials and methods

2.1. Materials

Melamine was purchased from the Tianjin Guangfu Fine Chemical Research Institute (Tianjing, China); potassium dichromate ($K_2Cr_2O_7$), AA, urea, glucose and thiourea of analytical grade from the Sinopharm Chemical Reagent Co., Ltd. (China); and the amino acids, GSH and uric acid from Sigma-Aldrich, Inc. (USA). Cr(VI) stock solution (20 mM) was prepared as follows: 294.2 mg $K_2Cr_2O_7$ (dried at 110 °C for 2 h) was dissolved in 10 mL water and then diluted in a 100-mL volumetric flask. AA stock solution (10 mM) was freshly prepared before experiments. Thioglycollic acid (TGA) was purchased from Aladin Ltd. (Shanghai, China). All chemicals were of analytical grade and used as received without further purification. Fetal bovine serum was purchased from Gibco, Inc. (USA); healthy human plasma was obtained from the First Affiliated Hospital of Xiamen University (Xiamen, China); kiwifruit juice was purchased from local supermarkets (Xiamen, China). Ultrapure water with a resistivity of 18.2 MΩ cm^{-1} obtained from a Millipore purification system (Millipore, USA) was used throughout the experiments. 50 mm × 0.22 μm water phase microporous membrane filters were purchased from Xiamen Green Reagent Glass Instrument Co., Ltd. (Xiamen, China).

2.2. Characterizations

UV−vis absorption spectra were obtained with a UV2550 UV−vis spectrophotometer (Shimadzu, Japan), and fluorescence spectra were performed using an F-4500 spectrophotometer (Hitachi, Japan). Quartz cuvette (H × W × D: 45 mm × 12.5 mm × 12.5 mm, optical path: 10 mm) was used for the absorption measurements and quartz fluorescence cuvette (H × W × D: 45 mm × 12.5 mm × 12.5 mm, optical path: 10 mm) was used for all the fluorescence measurements. All the quartz cuvettes were from Wuxi crystal and Optical Instrument Co., Ltd. (Wuxi, China). Fourier transform infrared (FT-IR) spectra were obtained on a Nicolet 330 spectrophotometer (Thermo Electron Corp., USA). The fluorescence lifetime was determined on a FluoroMax-4 spectrofluorometer (Horiba JobinYvon, France) and the excitation source was pulsed diode light source NanoLED-295 (peak wavelength: 297 nm, pulse duration < 1.0 ns, Horiba JobinYvon, France). Scanning electron microscope (SEM) images were collected with an LEO 1530 field-emission system S-4800 (Hitachi, Japan). Transmission electron microscope (TEM) images were collected using a TECNAI F-30 (Philips-FEI, Netherlands) at an acceleration voltage of 300 kV. Dynamic light scattering (DLS) and ζ-potential results were collected with a Nano-ZS (Malvern Instruments, UK). Atomic force microscopy (AFM) was performed on a 5500 SPM (Agilent, USA) with silicon probes. X-ray powder diffraction (XRD) results were collected with a Rigaku Ultima IV XRD diffractometer (Rigaku, Japan) equipped with graphite monochromatized high-intensity Cu-Kα radiation (λ = 1.5417 Å). X-ray photoelectron spectroscopy (XPS) measurements were performed on a PHI Quantum 2000 XPS system (Physical Electronics, USA) with Al Kα ($h\upsilon$ = 1486.60 eV) and all the binding energies were calibrated by C1s as reference energy (C1s = 284.8 eV). Inductively coupled plasma mass spectroscopy (ICP-MS) was performed with a DRC II 2000 ICP-MS instrument (PerkinElmer, USA).

2.3. Preparation of g-C_3N_4 nanosheets

G-C_3N_4 nanosheets were prepared based on the previous reports with minor modification (Chen et al., 2013; Zhang et al., 2013, 2014d). First, bulk g-C_3N_4 was prepared by heating 10.0 g melamine for 3 h to 550 °C and maintaining it at this temperature for 4 h in air. Nest, 1.0 g finely-ground bulk g-C_3N_4 powder was added into 100 mL 5 M HNO_3 and refluxed at 120 °C for 24 h. After natural cooling to room temperature, the refluxed product was centrifuged at 10,000 rpm for 30 min and then washed three times with ultrapure water to neutral. The remaining supernatant was collected and then given ultrasonic treatment for 16 h. The final solution of g-C_3N_4 nanosheets was gained by filtering the supernatant through a 50 mm × 0.22 μm water phase microporous membrane filter. The concentration of the as prepared g-C_3N_4 nanosheets was 250 μg/mL.

2.4. Fluorescence determination of Cr(VI) and AA

20 μL of the as-prepared solution of g-C_3N_4 nanosheets (5 μg/mL) was mixed with a 10 mM phosphate buffer solution (PBS, pH 4.0) containing different concentrations of Cr(VI). The final volume of the solution was kept as 1.0 mL. After mixing for 10 min at room temperature, the fluorescence spectra of the solutions were recorded.

In the determination of AA, 5 μg/mL g-C_3N_4 nanosheets was mixed with 10 mM PBS (pH 4.0) containing 2 mM Cr(VI) and different concentrations of AA, the final volume of the solution being 1.0 mL. The fluorescence spectra were recorded after reaction for 10 min at room temperature.

2.5. Selectivity measurements of Cr(VI) and AA

In the selectivity measurements of Cr(VI), several metal ions were selected as co-existing ions and used to investigate. The concentration of all ions was 200 μM. The concentration of the masking agent was selected as 1 mM, and the same detection conditions were selected as mentioned above. The multi-ions groups were some common co-existing ions in the environment. The concentration of each ion in the multi-ions groups was 200 μM.

In the selectivity measurements of AA, several co-existing substances were selected. The concentration of all substances was 200 μM in the solution containing 2 mM Cr(VI), and the same detection conditions were selected as mentioned above.

2.6. Time-resolved decay measurements

To test the mechanism between g-C_3N_4 nanosheets and Cr(VI), time-resolved decay measurements of the as prepared g-C_3N_4 nanosheets (0, 2, 20, 100 and 200 μM) were detected in 10 mM PBS (pH 4.0).

2.7. Determination of Cr(VI) in lake water samples and AA in biological fluids samples

The lake water samples were obtained from Xiamen University campus. Lake water and kiwifruit juice were centrifuged at 12,000 rpm for 20 min and then the supernatant filtered through the 0.22 μm water phase membrane to obtain the samples. To avoid the interferences to pH in the determination of AA in biological fluids samples, the fetal bovine serum, healthy human plasma and kiwifruit juice samples were diluted 30-fold in 10 mM PBS (pH 4.0). In the determination of Cr(VI), 5 μg/mL g-C_3N_4 nanosheets was injected into 10 mM PBS (pH 4.0) solution containing a 0.5 mL water sample and different concentrations of Cr(VI). And in the determination of AA, 5 μg/mL g-C_3N_4 nanosheets was injected into 10 mM PBS (pH 4.0) solution containing 2 mM Cr(VI) and 100 μL diluted biological fluids. The final volume of the solution was 1 mL. The fluorescence spectra of the solutions were collected after reaction for 10 min at room temperature for the determination of Cr(VI) and AA.

3. Results and discussion

3.1. Materials characterization

As is known, g-C_3N_4 with atomic-scale thickness and nanoscale size can greatly promote the photoresponse and electroresponse compare with bulk materials (Li and Lin, 2006; Niu et al., 2012; Yang et al., 2013). The morphologies of the bulk g-C_3N_4 and the g-C_3N_4 nanosheets were observed using SEM and TEM. As shown in Fig. 1A, for bulk g-C_3N_4, the rocky-like structure consists of irregular folded flakes with a size of several micrometers. In contrast to the bulk g-C_3N_4, from the TEM image, the g-C_3N_4 nanosheets were much thinner and smaller, with a mean diameter of 70 nm (Fig. 1B). AFM was used to further investigate the structural features of g-C_3N_4 nanosheets (Fig. 1C). The thickness of the g-C_3N_4 nanosheets was demonstrated to be 2.13 nm (Fig. 1D), indicating that the as prepared g-C_3N_4 nanosheets comprised less than seven C–N layers, which was similar to previous reports (Chen et al., 2013; Zhang et al., 2014d). Different from the bulk g-C_3N_4, the as prepared g-C_3N_4 nanosheets could be very well dispersed in water. The solution was nearly transparent and could remain stable in storage at 4 °C for six months without aggregation (Fig. S1). The Tyndall phenomenon of the as prepared g-C_3N_4 nanosheets indicated their good monodispersity in water (Fig. S1). In addition, the DLS and ζ-potential results revealed a mean hydrated radius of 80.4 nm and a zeta potential of 14.0 mV for the as prepared g-C_3N_4 nanosheets (Figs. S2 and S3), and these results also indicated the good dispersibility and stability of g-C_3N_4 nanosheets.

XRD patterns of the bulk g-C_3N_4 and the g-C_3N_4 nanosheets are shown in Fig. S4. For the bulk g-C_3N_4, the strong XRD Bragg peak was centered at 27.3° (d=0.327 nm) corresponding to the characteristic interlayer stacking reflection of conjugated aromatic system, indexing for graphitic materials as the (002) peak (Wang et al., 2009). The small XRD peak at 13.0° (d=0.681 nm) corresponded to the diffraction at a periodic in-planar structural packing feature within the sheets (Zhang et al., 2014a). The low-angle peak at 13.0° nearly disappeared owing to the simultaneously decreased planar size of the layers during the chemical oxidization and liquid exfoliation. Meanwhile, the intensity of the (002) peak significantly decreased, the peak width increased and the peak had a slight red shift to 27.7° (d=0.322 nm). The decrease

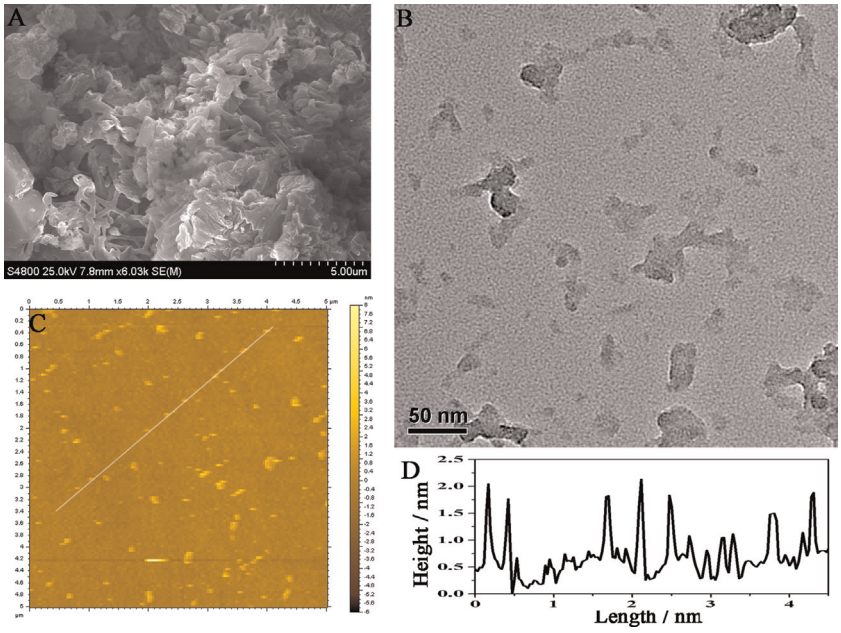

Fig. 1. (A) SEM image of the bulk g-C_3N_4; (B) TEM image of the g-C_3N_4 nanosheets; (C) AFM image of the g-C_3N_4 nanosheets; and (D) the height of g-C_3N_4 nanosheets.

in the interplanar stacking distance from 0.327 nm to 0.322 nm demonstrated that the layered g-C_3N_4 was successfully exfoliated into nanoscale layer structures as expected (Yang et al., 2013; Zhang et al., 2014a). XPS and FT-IR measurements were performed to explore the chemical composition of the bulk g-C_3N_4 and the g-C_3N_4 nanosheets (Figs. S5 and S6). As shown in Figs. S5A and S5D, the C/N/O atomic concentration ratio of the bulk g-C_3N_4 and the g-C_3N_4 nanosheets were 0.450/0.515/0.0355 and 0.515/0.199/0.287. The oxygen content increase in the g-C_3N_4 nanosheets may have been caused by amino functional groups in the bulk g-C_3N_4 nucleus decomposing into oxygen-containing groups during the chemical oxidation and liquid exfoliation, which is similar to the mechanism in hydrothermal treated fluorescent g-C_3N_4 (Zhang et al., 2014b). C1s spectrum of both bulk g-C_3N_4 and g-C_3N_4 nanosheets showed two peaks centered at 284.8 eV and 288.5 eV, attributed to graphitic carbon and the sp^2-bonded carbon (N–C=N). In the N1s spectrum of the bulk g-C_3N_4, three peaks occurred, centered at 398.7 eV, 399.7 eV and 400.0 eV, and similarly for the g-C_3N_4 nanosheets at 398.6 eV, 399.7 eV and 400.7 eV. The major peaks at 398.7 eV and 398.6 eV corresponded to sp^2 hybridized aromatic nitrogen bonded to carbon atoms (C=N–C). The peak at 399.7 eV could be ascribed to the tertiary nitrogen bonded to carbon atoms (N–(C)3) or (H–N–(C)2). The peaks at 400.0 eV and 400.7 eV were attributed to quaternary nitrogen bonded three carbon atoms in the aromatic cycles (Tang et al., 2013). As shown in Fig. S6, in the FT-IR experiments, both the bulk g-C_3N_4 and the g-C_3N_4 nanosheets exhibited typical graphite carbon nitride peaks. The peaks between 3000 cm^{-1} and 3600 cm^{-1} represented N–H stretching and hydrogen-bonding interactions. The peaks between 1100 cm^{-1} and 1800 cm^{-1} corresponded to the characteristic stretching modes of CN heterocycles, full condensation of C–N(–C)–C and partial condensation of C–NH–C. The peak at 810 cm^{-1} was attributed to the vibration of the triazine ring (Yang et al., 2013; Zhang et al., 2013). From the results, it was obvious that the g-C_3N_4 nanosheets remained mainly as the structure of the bulk g-C_3N_4 after chemical oxidation and liquid exfoliation.

In the experiments, we found that the strong fluorescence of the g-C_3N_4 nanosheets could be efficiently turned off in the presence of Cr(VI) owing to the IFE. Since there is a good spectral overlap between the absorption band of Cr(VI) and the excitation and emission wavelength of the g-C_3N_4 nanosheets. The strong IFE can quench the fluorescence of the g-C_3N_4 nanosheets efficiently. Meanwhile, the fluorescence would be turned on again owing to the weakened IFE caused by the oxidation–reduction between Cr (VI) and AA. The reductant AA can react with the antioxidant Cr (VI) to form Cr(III) and (dehydroascorbic acid) DAA. The possible process for the phenomena is illustrated in Scheme 1.

3.2. Spectroscopic properties of g-C_3N_4 nanosheets

In order to reveal the analytical performances of the g-C_3N_4 nanosheets, the UV–vis absorption and fluorescence emission spectra of the g-C_3N_4 nanosheets were studied. As displayed in Fig. 2A, a strong absorption peak at 310 nm and a shoulder peak at 365 nm could be found. Under an excitation wavelength of 310 nm, the solution of g-C_3N_4 nanosheets exhibited a strong emission peak at a wavelength of 438 nm, indicating a 33 nm blue shift compared with the 471 nm emission wavelength of the bulk g-C_3N_4. The shift was caused by the quantum confinement effect (Zhang et al., 2013). As shown in Fig. 2B, there was only one emission peak at a wavelength of 438 nm when the excitation wavelength was changed from 290 to 370 nm, and the maximum emission intensity could be obtained at an excitation wavelength of 310 nm. The constant emission wavelength indicated that the as prepared solution of g-C_3N_4 nanosheets contained a single emitter only. Measurement of the g-C_3N_4 nanosheets showed their high photostability with the fluorescence intensity remaining constant after continuous irradiation for 2 h (Fig. S7). The stability of g-C_3N_4 nanosheets was investigated in the presence of various concentrations of NaCl and the fluorescence intensity of the g-C_3N_4 nanosheets remained constant even in 1 M NaCl solution compared with that without NaCl (Fig. S8), revealing the potential applications of the g-C_3N_4 nanosheets in high ionic strength environments. The relative quantum yield of the as prepared g-C_3N_4 nanosheets was 5.50% in reference to quinoline sulfate (QY 54% at 360 nm excitation).

In the inner filter effect (IFE), it is necessary that there is a good spectral overlap between the absorption band of a quencher and the excitation and/or emission wavelength of a fluorescent agent. As illustrated in Fig. S9, Cr(VI) exhibited three broad absorption

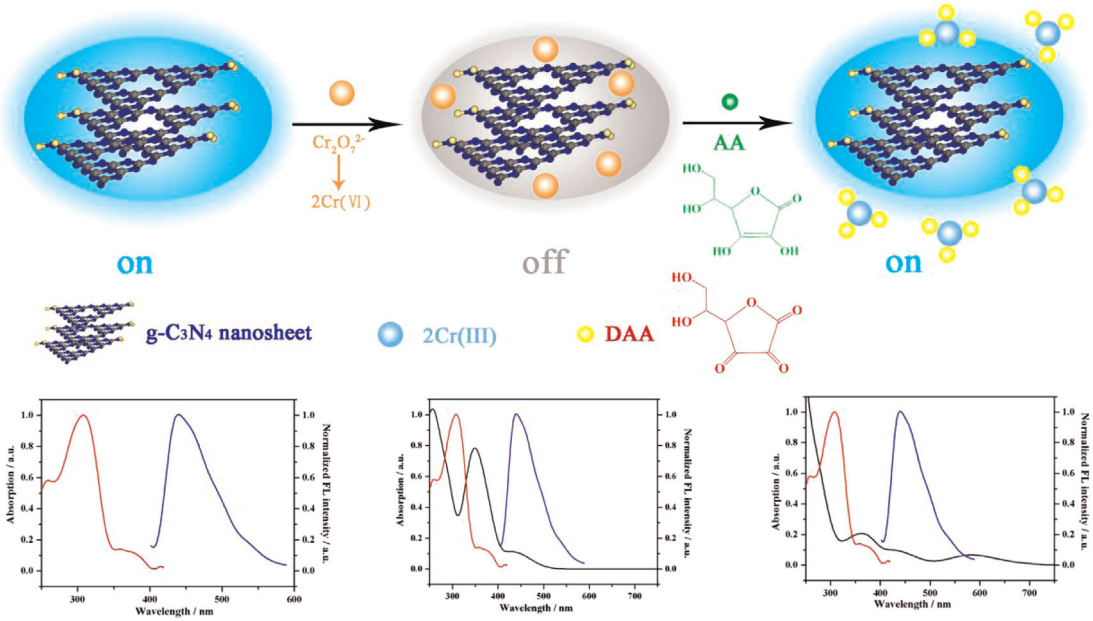

Scheme 1. Schematic illustration of fluorescence "on–off" assay for Cr(VI) and "on–off–on" assay for AA.

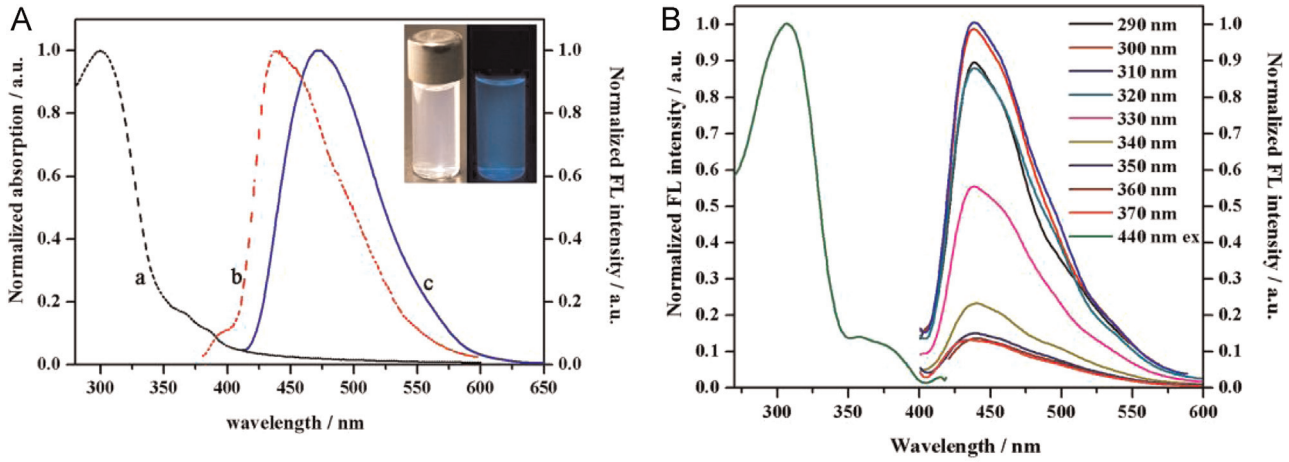

Fig. 2. (A) UV–vis absorption (a) and the fluorescence emission spectra (b) of the g-C_3N_4 nanosheets, and the fluorescence emission spectra (c) of the bulk g-C_3N_4. Inset: the photographs of the solution of g-C_3N_4 nanosheets under daylight (left) and 365 nm UV light (right). (B) The fluorescence excitation spectrum and the emission spectra of g-C_3N_4 nanosheets under different excitation wavelength ranging from 290 to 370 nm.

peaks at 260, 360 and 440 nm. In the meantime, the as prepared solution of g-C_3N_4 nanosheets showed a broad excitation wavelength at 310 nm and an emission wavelength centered at 438 nm. Therefore, we explored the feasibility of using the as prepared solution of g-C_3N_4 nanosheets for the determination of Cr(VI). As expected, the addition of Cr(VI) led to a measurable fluorescence intensity decrease in the solution of g-C_3N_4 nanosheets.

3.3. Optimization of the reaction conditions

To achieve the sensitive detection of Cr(VI), the effects of pH value and the amount of g-C_3N_4 nanosheets on the fluorescence intensity were investigated. As shown in Fig. S10, the fluorescence intensity of the solution of g-C_3N_4 nanosheets-Cr(VI) decreased with pH increase from 2 to 12, but the change of fluorescence intensity was almost negligible in the pH range 2–4. Considering the absorption spectrum of Cr(VI) and the fluorescence characteristics of the g-C_3N_4 nanosheets in various pH solutions, we chose a mild condition at the pH value of 4. The results in Fig. S11 indicate that the maximum fluorescence was observed when 5 μg/mL g-C_3N_4 nanosheets was applied. Furthermore, to optimize the analytical procedure, the effect of reaction time between the g-C_3N_4 nanosheets and the Cr(VI) was also investigated. Upon the addition of 2 mM Cr(VI) solution into the solution of g-C_3N_4 nanosheets, a rapid equilibration for the reaction could be achieved in 10 min. Therefore, the following experiments were carried out under the same conditions: 1.0 mL reaction solution containing 5 μg/mL g-C_3N_4 nanosheets in 10 mM PBS (pH 4.0), a reaction time of 10 min, with a 310 nm fluorescence excitation wavelength.

3.4. Fluorescence determination of Cr(VI) and AA

The analytical performance of the g-C_3N_4 nanosheets was evaluated. In this sensitivity study, different concentrations of Cr (VI) in the range 0–6 mM were investigated. Fig. 3A shows that the fluorescence intensity at 438 nm gradually decreased with the increase of Cr(VI) concentration, even at a low concentration of 50 nM, which revealed that the fluorescence intensity of the g-C_3N_4 nanosheets was sensitive to the concentration change of Cr (VI). The fluorescence spectra as presented in Fig. 3B indicate that there is a good linearity between the florescence intensity and the Cr(VI) concentration ranging from 0.6 to 300 μM, with a limit of detection (LOD) of 0.15 μM at a signal-to-noise ratio of 3. The fluorescence intensity versus the concentration of Cr(VI) could be

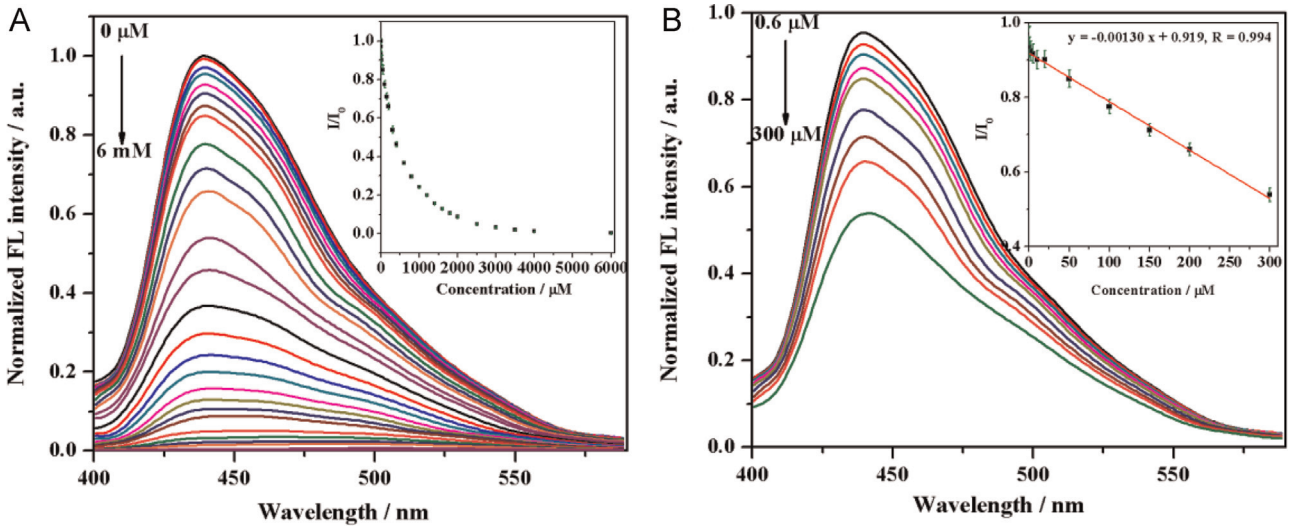

Fig. 3. (A) Fluorescence responses of the g-C_3N_4 nanosheets in the presence of different concentration of Cr(VI). The inset figure presents the relationship between I/I_0 and the concentration of Cr(VI). (B) Fluorescence responses of the g-C_3N_4 nanosheets in the presence of different concentrations of Cr(VI) within the linear range. The inset figure presents the linear range of I/I_0 and the concentrations of Cr(VI), with I_0 and I being the fluorescence intensities at 438 nm in the absence and presence of Cr(VI).

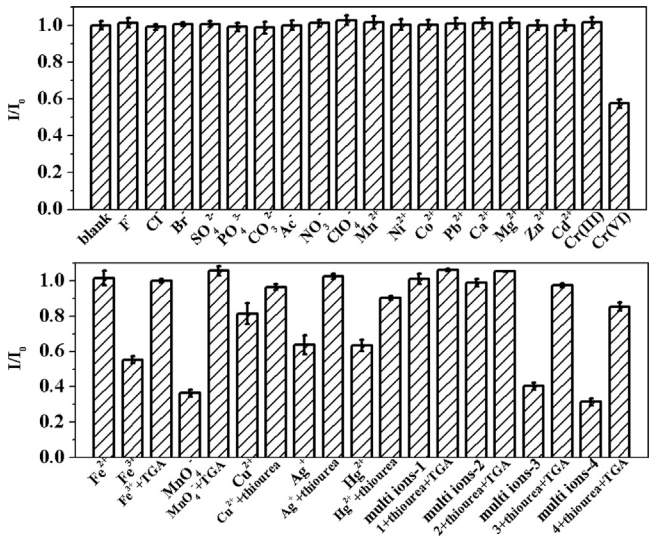

Fig. 4. Fluorescence responses of the g-C_3N_4 nanosheets in the presence of 200 μM solution of various ion. The blank represents the fluorescence responses of the solution of g-C_3N_4 nanosheets without any ion. The multi-ions-1 contains Ca^{2+}, Mg^{2+}, K^+, Na^+; multi-ions-2 contains F^-, Cl^-, Br^-, SO_4^{2-}, PO_4^{3-}, CO_3^{2-}, Ac^-, NO_3^-;multi-ions-3 contains Mn^{2+}, Cu^{2+}, Ni^{2+}, Fe^{3+}, Zn^{2+}, Co^{2+}; multi-ions-4 contains Cu^{2+}, Fe^{2+}, Fe^{3+}, Hg^{2+}, the concentration of each ion in the multi-ions groups was 200 μM.

fitted into a linear equation: $I/I_0 = -0.00130[Cr(VI)]$ (μmol/L)+ 0.919, with a correlation coefficient R of 0.994. According to the US Environmental Protection Agency, the maximum concentration of Cr(VI) in drinking water should be less than 0.1 mg/L (1.9 μM) (Li et al., 2011), indicating that the proposed approach is sensitive enough to monitor Cr(VI) levels in drinking water.

In order to evaluate selectivity, the effects of the co-existing ions were investigated under the same conditions. The results in Fig. 4 indicate that 200 μM Cu^{2+}, Ag^+, Hg^{2+} or Fe^{3+} presented an obviously quenching effect on the fluorescence of the g-C_3N_4 nanosheets due to their chelation with N atoms in the g-C_3N_4 nanosheets (Barman and Sadhukhan, 2012; Tang et al., 2013; Tian et al., 2013a; Zhang et al., 2014b). In order to exclude such interferences, thiourea was used as an efficient masking reagent. Fig. 4 shows that the interference of Cu^{2+} and Ag^+ could be obviously reduced in the presence of 1 mM thiourea, with Hg^{2+} still exhibiting a small influence and Fe^{3+} could be reduced in the presence of 1 mM TGA. MnO_4^- is the major interference ion which has a wide absorption range across from the UV to the visible region (Fig. S13), but MnO_4^- can be easily removed by adding 1 mM TGA because of its strong oxidizing property. These results revealed that g-C_3N_4 nanosheets were relatively selective towards Cr(VI). A fluorescence change for the co-existing ions in the solution of 200 μM Cr(VI) and the g-C_3N_4 nanosheets were also detected and the results are shown in Fig. S14. It was obvious that reducibility ions would affect the quenching efficiency of Cr(VI) towards the fluorescence of the g-C_3N_4 nanosheets owing to a decreased concentration of Cr(VI) caused by its reduction into Cr(III).

Considering the IFE process between the g-C_3N_4 nanosheets and Cr(VI), as well as the strongly oxidative property of Cr(VI) under acidic condition, we proposed the possibility of sensing some strong reductant via a fluorescence "on–off–on" process. AA is an important antioxidant which plays a vital role in our daily life (Hernández et al., 2006; Li and Lin, 2006), it is also a reductant which is used for removing Cr(VI) (Xu et al., 2004). Fig. 5A reveals that the fluorescence of the solution of g-C_3N_4 nanosheets was recovered with the addition of AA. Fig. 5B shows that there is a good linearity between the fluorescence intensity and the concentration of AA ranging from 0.5 to 200 μM, with an LOD of 0.13 μM. The fluorescence intensity versus the concentration of AA could be fitted into a linear equation: $I/I_0 = 0.00152$ [AA] (μmol/L)+1.07 (R=0.995). After a reaction time of 10 min, the fluorescence intensity reached at its 98% maximum value (Fig. S15).

To evaluate the selectivity of the solution of g-C_3N_4 nanosheets-Cr(VI) as a fluorescence on–off–on system for the determination of AA, the effects of the co-existing substances were investigated under the same conditions. As seen in Fig. S16, the restored fluorescence due to 200 μM AA was much more obvious than other co-existing substances.

3.5. Discussion on the mechanism involved in the determination of Cr(VI) and AA

In order to further verify the selectivity mechanism of the g-C_3N_4 nanosheets towards Cr(VI), we explored the fluorescence lifetime of the g-C_3N_4 nanosheets with several different concentrations of Cr(VI). As shown in Fig. S17, the lifetime remained constant under 297 nm excitation, and the florescence decay of the g-C_3N_4 nanosheets was fitted using a three-exponential decay function to yield a lifetime of 4.8 ns. The results fully confirmed the IFE mechanism of the "on–off" fluorescence response in the determination of Cr(VI) using g-C_3N_4 nanosheets, rather than

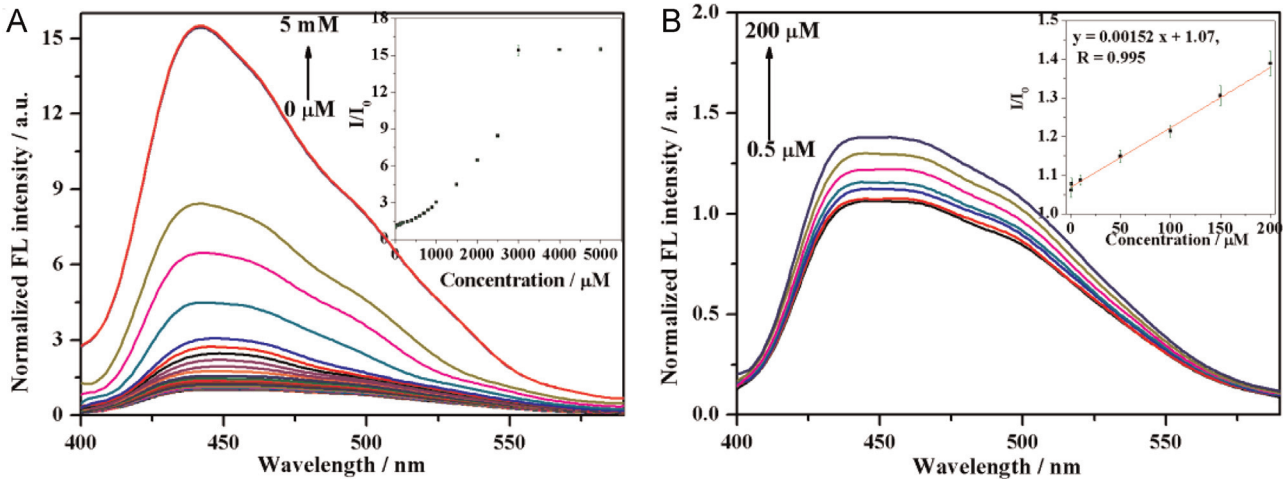

Fig. 5. (A) Fluorescence responses of the g-C_3N_4 nanosheets in the presence of 2 mM Cr(VI) and different concentrations of AA. The inset figure presents the relationship between I/I_0 and the concentrations of AA. (B) Fluorescence responses of the g-C_3N_4 nanosheets in the presence of 2 mM Cr(VI) and different concentrations of AA within the linear range. The inset figure presents the linear range of I/I_0 and the concentrations of AA.

fluorescence resonance energy transfer. To figure out the mechanism of the g-C_3N_4 nanosheets-Cr(VI) towards AA, we detected the absorption spectra of g-C_3N_4 nanosheets-Cr(VI) in different concentrations of AA. As shown in Fig. S18, the absorption spectra of Cr(VI) at 353 nm gradually decreased with the increase of AA, while the absorption spectra of Cr(III) at 587 nm appeared and increased with the increase of AA. The absorption spectra indicated that Cr(VI) can be reduced into Cr(III) by AA, which is similar to a previous report (Xu et al., 2004), the absorption spectrum of g-C_3N_4 nanosheets was almost unchanged during the whole process. The changed absorption spectra of Cr lowered the efficiency of IFE owing to the oxidation–reduction between Cr(VI) and AA. At the same time, it could be clearly seen in Fig. S19 that the influence of AA to fluorescence of g-C_3N_4 nanosheets is negligible. All in all, the proposed sensing approach provides the obvious advantages of simplicity, convenience, economical cost and rapid implementation.

3.6. Determination of Cr(VI) in lake water samples and AA in biological fluids samples

The applicability of the proposed method was tested in the determination of Cr(VI) in lake water samples. A recovery study was carried out on the samples spiked with standard Cr(VI) solutions (2, 20 and 200 μM) to evaluate the method we developed. The obtained recoveries of the samples varied from 93.6% to 106%, and the detection results agreed well with those obtained from ICP-MS, suggesting the applicability of the proposed method to lake water samples (Table S1).

The applicability of the proposed method was also tested in the determination of AA in biological fluids samples. The concentration of AA in the diluted fetal bovine serum, human plasma and kiwifruit juice determined by our method was 0.907, 0.695 and 2.67 μM, respectively. A recovery study was also carried out on the samples spiked with standard AA solutions (5, 50 and 150 μM) to evaluate the method we developed. The obtained recoveries of the samples varied from 96.3% to 102%, suggesting the applicability of the proposed method to biological fluids samples (Table S2). We also compared our method to other methods of Cr(VI) and AA detection (Table S3 and S4), the determination of both them of is rare. Although the LOD of our method is not the lowest for either Cr(VI) or AA, the simplicity and the capability for detection of both of them are the obvious advantages over other methods.

4. Conclusions

In summary, we developed an efficient florescence approach using g-C_3N_4 nanosheets for the determination of Cr(VI) and AA. The method was applied in the determination of Cr(VI) in lake waters and AA in biological fluids. The fluorescence intensity of the g-C_3N_4 nanosheets would be turned off in the presence of Cr (VI) because of the IFE, while the fluorescence intensity would recover with the subsequent addition of AA via the oxidation–reduction between Cr(VI) and AA. Relying on the IFE, more fluorescence sensing based on g-C_3N_4 nanosheets can be developed in the future.

Acknowledgments

This research was financially supported by the National Nature Scientific Foundation of China (Nos. 21175112 and 21375112) and the National Basic Research Program of China (2010CB732402) and the program of Science and Technology of Xiamen for University Innovation (3502Z20143025), which are gratefully acknowledged. Furthermore, we would like to extend our thanks to Professor John Hodgkiss of The University of Hong Kong for his assistance with English.

Appendix A. Supplementary material

Supplementary data associated with this article can be found in the online version at http://dx.doi.org/10.1016/j.bios.2014.12.024.

References

Arancibia, V., Valderrama, M., Silva, K., Tapia, T., 2003. J. Chromatogr. B 785 (2), 303–309.
Balasubramanian, S., 1999. Talanta 50 (3), 457–467.
Barman, S., Sadhukhan, M., 2012. J. Mater. Chem. 22 (41), 21832–21837.
Broadhurst, C.L., Domenico, P., 2006. Diabetes Technol. Ther. (8 6), 677–687.
Chen, L., Huang, D., Ren, S., Dong, T., Chi, Y., Chen, G., 2013. Nanoscale 5 (1), 225–230.
Chen, Y.J., Yan, X.P., 2009. Small 5 (17), 2012–2018.
Cheng, C., Huang, Y., Wang, J., Zheng, B., Yuan, H., Xiao, D., 2013. Anal. Chem. 85 (5), 2601–2605.
Cheng, C., Huang, Y., Tian, X., Zheng, B., Li, Y., Yuan, H., Xiao, D., Xie, S., Choi, M.M., 2012. Anal. Chem. 84 (11), 4754–4759.
Chwastowska, J., Skwara, W., Sterlinska, E., Pszonicki, L., 2005. Talanta 66 (5), 1345–1349.
Han, Z., Qi, L., Shen, G., Liu, W., Chen, Y., 2007. Anal. Chem. 79 (15), 5862–5868.
Hernández, Y., Lobo, M.G., González, M., 2006. Food Chem. 96 (4), 654–664.
Hosseini, M., Gupta, V.K., Ganjali, M.R., Rafiei-Sarmazdeh, Z., Faridbod, F., Goldooz, H., Badiei, A.R., Norouzi, P., 2012. Anal. Chim. Acta 715, 80–85.
Hou, Y., Zuo, F., Dagg, A.P., Liu, J., Feng, P., 2014. Adv. Mater. 26 (29), 5043–5049.
Huang, H., Yang, S., Vajtai, R., Wang, X., Ajayan, P.M., 2014. Adv. Mater. 26 (30), 5160–5165.
Ishii, K., Kubo, K., Sakurada, T., Komori, K., Sakai, Y., 2011. Chem. Commun. 47 (17), 4932–4934.
Jahan, S., Mansoor, F., Kanwal, S., 2014. Biosens. Bioelectron. 53, 51–57.
Jin, W., Wu, G., Chen, A., 2014. Analyst 139 (1), 235–241.
Lee, E.Z., Jun, Y.S., Hong, W.H., Thomas, A., Jin, M.M., 2010. Angew. Chem. Int. Ed. 49 (50), 9706–9710.
Li, F.-M., Liu, J.-M., Wang, X.-X., Lin, L.-P., Cai, W.-L., Lin, X., Zeng, Y.-N., Li, Z.-M., Lin, S.-Q., 2011. Sensor Actuat. B—Chem. 155 (2), 817–822.
Li, N., Li, Y., Han, Y., Pan, W., Zhang, T., Tang, B., 2014. Anal. Chem. 86 (8), 3924–3930.
Li, Y., Lin, X., 2006. Sensor Actuat. B—Chem. 115 (1), 134–139.
Li, Y., Zhang, H., Liu, P., Wang, D., Zhao, H., 2013. Small 9 (19), 3336–3344.
Lin, L.-S., Cong, Z.-X., Li, J., Ke, K.-M., Guo, S.-S., Yang, H.-H., Chen, G.-N., 2014a. J. Mater. Chem. B 2 (8), 1031.
Lin, T., Zhong, L., Wang, J., Guo, L., Wu, H., Guo, Q., Fu, F., Chen, G., 2014b. Biosens. Bioelectron. 59, 89–93.
Ma, T.Y., Dai, S., Jaroniec, M., Qiao, S.Z., 2014a. Angew. Chem. Int. Ed. 53 (28), 7281–7285.
Ma, W., Han, D., Zhou, M., Sun, H., Wang, L., Dong, X., Niu, L., 2014b. Chem. Sci. 5, 3946–3951.
Malashikhina, N., Pavlov, V., 2012. Biosens. Bioelectron. 33 (1), 241–246.
Niu, P., Zhang, L.L., Liu, G., Cheng, H.M., 2012. Adv. Funct. Mater. 22 (22), 4763–4770.
Rattanarat, P., Dungchai, W., Cate, D.M., Siangproh, W., Volckens, J., Chailapakul, O., Henry, C.S., 2013. Anal. Chim. Acta 800, 50–55.
Ravindran, A., Elavarasi, M., Prathna, T.C., Raichur, A.M., Chandrasekaran, N., Mukherjee, A., 2012. Sensor Actuat. B—Chem. 166-167, 365–371.
Ščančar, J., Milačič, R., 2014. J. Anal. Atom. Spectrom. 29 (3), 427.
Sedman, R.M., Beaumont, J.A.Y., McDonald, T.A., Reynolds, S., Krowech, G., Howd, R., 2006. J. Environ. Sci. Health C 24 (1), 155–182.
Sun, J., Zhang, J., Jin, Y.D., 2013. J. Mater. Chem. C 1 (1), 138–143.
Tang, Y., Song, H., Su, Y., Lv, Y., 2013. Anal. Chem. 85 (24), 11876–11884.
Tang, Y., Su, Y., Yang, N., Zhang, L., Lv, Y., 2014. Anal. Chem. 86 (9), 4528–4535.
Tian, J., Liu, Q., Asiri, A.M., Al-Youbi, A.O., Sun, X., 2013a. Anal. Chem. 85 (11), 5595–5599.
Tian, J., Liu, Q., Asiri, A.M., Qusti, A.H., Al-Youbi, A.O., Sun, X., 2013b. Nanoscale 5 (23), 11604–11609.
Tian, J., Liu, Q., Ge, C., Xing, Z., Asiri, A.M., Al-Youbi, A.O., Sun, X., 2013c. Nanoscale 5 (19), 8921–8924.
Wang, H.J., Du, X.M., Wang, M., Wang, T.C., Ou-Yang, H., Wang, B., Zhu, M.T., Wang, Y., Jia, G., Feng, W.Y., 2010. Talanta 81 (4–5), 1856–1860.
Wang, X., Maeda, K., Thomas, A., Takanabe, K., Xin, G., Carlsson, J.M., Domen, K., Antonietti, M., 2009. Nat. Mater. 8 (1), 76–80.
Xu, H., Yan, J., She, X., Xu, L., Xia, J., Xu, Y., Song, Y., Huang, L., Li, H., 2014. Nanoscale 6 (3), 1406–1415.
Xu, J., Zhang, L., Shi, R., Zhu, Y., 2013. J. Mater. Chem. A 1 (46), 14766.
Xu, X.R., Li, H.B., Li, X.Y., Gu, J.D., 2004. Chemosphere 57 (7), 609–613.
Yang, S., Gong, Y., Zhang, J., Zhan, L., Ma, L., Fang, Z., Vajtai, R., Wang, X., Ajayan, P.M.,

2013. Adv. Mater. 25 (17), 2452–2456.
Zhang, J., Zhang, M., Yang, C., Wang, X., 2014a. Adv. Mater. 26 (24), 4121–4126.
Zhang, S., Li, J., Zeng, M., Xu, J., Wang, X., Hu, W., 2014b. Nanoscale 6 (8), 4157–4162.
Zhang, X., Wang, H., Zhang, Q., Xie, J., Tian, Y., Wang, J., Xie, Y., 2014c. Adv. Mater. 26 (26), 4438–4443.
Zhang, X., Xie, X., Wang, H., Zhang, J., Pan, B., Xie, Y., 2013. J. Am. Chem. Soc. 135 (1), 18–21.
Zhang, X.L., Zheng, C., Guo, S.S., Li, J., Yang, H.H., Chen, G., 2014d. Anal. Chem. 86 (7), 3426–3434.
Zhao, L., Jin, Y., Yan, Z., Liu, Y., Zhu, H., 2012. Anal. Ch im. Acta 731, 75–81.
Zheng, M., Xie, Z., Qu, D., Li, D., Du, P., Jing, X., Sun, Z., 2013. ACS Appl. Mater. Interface 5 (24), 13242–13247.
Zhu, Y.P., Li, M., Liu, Y.L., Ren, T.Z., Yuan, Z.Y., 2014. J. Phys. Chem. C 118 (20), 10963–10971.